Plasmon structure in the x-ray absorption spectra of metals

Shyamalendu M. Bose* and Pierre Longe
Institut de Physique, Université de Liège, Sart-Tilman, B-4000 Liège, Belgium
(Received 23 January 1978)

The effect of plasmon production on the x-ray photoabsorption spectra of metals has been studied in the framework of the many-body perturbation theory. The plasmon starts to contribute very weakly at the frequency $E_F + \omega_p^o$ (E_F is the absorption-edge frequency and ω_p^o is the frquency of a zero-momentum plasmon). The plasmon absorption edge at this frequency is, in fact, so weak that it does not have any significant effect on the calculated spectrum and possibly cannot be detected. However, a new structure appears at a higher frequency. This structure occurs as a dip of 5%–7% at the frequency $E_F + \omega_p^c$ where ω_p^c is the highest frequency of the plasmon dispersion curve beyond which plasmon production is precluded. The physical significance of $E_F + \omega_p^c$ is that it is the lowest x-ray frequency at which the plasmon excitation can become a real process during x-ray photoabsorption in metals. The existence of the plasmon structure at this frequency allows an estimation of the extent of plasmon dispersion in metals.

I. INTRODUCTION

For the past few decades there has been a great deal of interest in the prediction and observation of various elementary excitations (e.g., plasmons, magnons, polarons, etc.) in solids. The effect of plasmon excitation in a metal is demonstrated in many of its electronic and optical properties. For example, the production of a plasmon during the soft-x-ray emission of a metal has been studied quite extensively both theoretically[1–4] and experimentally.[5,6] A weak satellite band is found to occur on the low-energy side (tailing region) of the spectrum, shifted by an energy ω_p (classical plasma frequency) from the high-energy edge of the emission spectrum.

The effect of the plasmon production of the x-ray photoabsorption spectra of a metal is not so well known. Normally one would expect to observe a plasmon satellite absorption edge at a frequency ω_p above the frequency E_F corresponding to the absorption of edge of a metal. However, so far nothing significant has been observed[7] at this frequency. The reason for this may lie in any or all of the following three arguments. First, the satellite edge may be weaker in absorption than in emission as shown by the calculations of Bergersen *et al.*[8] In other words, the cancellation effects responsible for making the intensity of the emission satellite weak, may be evan stronger for the absorption satellite. Secondly, the slope at the satellite edge is less steep than that of the main absorption edge because of dispersion of the plasmon frequency. Finally the band-structure effects play a much more important role at the absorption frequencies and may make the weak satellite edge completely obscure.

However, it turns out that the effect of the plasmon production can become more important at a somewhat higher frequency, $E_F + \omega_p(k_c)$ where [due to the plasmon dispersion relation $\omega = \omega_p(k)$] k_c and $\omega_p(k_c)$ are the wave number and frequency beyond which the plasmon dispersion curve merges into the single-particle excitation region of the ω-k plane[9] (see Fig. 2). Calling $\omega_p^0 \equiv \omega_p(0)$ and $\omega_p^c \equiv \omega_p(k_c)$, it is interesting to note, in this regard, that the ratio ω_p^c/ω_p^0 is practically constant over the whole range of electron densities for the usual metals (the ratio varies between 1.50 for $r_s = 2$ and 1.48 for $r_s = 5$). Thus, once the classical plasma frequency ω_p^0 is known, $E_F + \omega_p^c$ for any metal can be readily estimated.

At this frequency, a new structure appears, which, to our knowledge, has not been reported before. This structure occurs as a dip of a few percent and extends over a frequency range of one or two eV, in the intensity of the x-ray photoabsorption spectra of metals. The magnitude and shape of this structure are not significantly different in the absorption band of most metals. Most recently, attempts have been made by Sénémaud[10] and she has been successful in observing a weak structure at the predicted frequencies in the K spectra of Al and Mg (following paper).

In the next section, the physical origin of this plasmon structure will be discussed. It will be interpreted by the combination of two reasons, namely the discontinuity of the Fermi distribution and the possibility of producing plasmons with conservation of energy in the intermediate state when the frequency is higher than $E_F + \omega_p^c$. In Sec. III, a qualitative approach to determine the shape of the structure in terms of a formal model of excitation of a plasmon mode with a single wave vector $\vec{k}$ will be presented. In Sec. IV, a calculation in a realistic model of the x-ray photoabsorption

spectra of metals will be performed in the first order of effective electron-electron potential. Conclusions will be drawn in Sec. V.

II. ORIGIN OF THE STRUCTURE AT $E_F + \omega_p^c$

In this section, we present physical arguments for why one should expect a plasomon structure at the frequency $E_F + \omega_p^c$. Consider, for the simplicity of argument, the x-ray absorption spectrum of an ideal metal where the band-structure effects can be ignored. As shown in Fig. 1, three frequencies can be distinguished in which the photoabsorption presents a different character with regard to plasmon excitation. Figure 1(a) represents the photoabsorption close to frequency E_F (absorption edge). A core electron of energy ϵ_B absorbs the incoming photon of energy $E_F \approx \epsilon_F - \epsilon_B$ and jumps just above the Fermi level ϵ_F. Due to the lack of extra energy of the photon, this transition cannot be accompanied by any plasmon production. This situation occurs up to frequency $E_F + \omega_p^0$ which is the lowest frequency where a plasmon can be excited. This will be the frequency of a possible satellite edge. This situation is represented in Fig. 1(b). The core electron is finally accomodated close to the Fermi edge via an intermediate transition through a state of higher energy $E_F + \omega_p^0$. The plasmon is produced in the intermediate state and the electron drops from state $\epsilon_F + \omega_p^0$ to state ϵ_F. We will see that this transition is necessarily virtual (no energy conservation between the intermediate state and the final state). To have such conservation of energy, we need a photon of higher energy and this energy will be shown to be precisely $E_F + \omega_p^c$. Figure 1(c) represents this third situation where the core electron is once more accomodated close to the Fermi level in the final state, but the intermediate state now has sufficient energy to yield a plasmon by a real or extrinsic process, i.e., a process where energy is conserved.

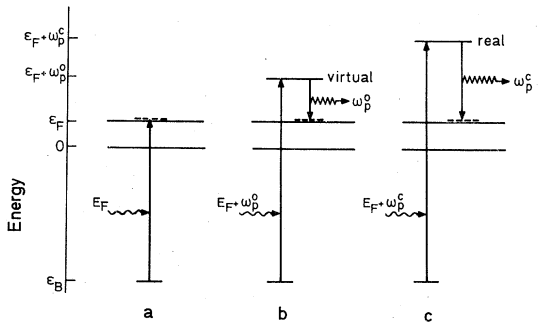

FIG. 1. X-ray photoabsorption process in a metal. (a) Represents photoabsorption without any plasmon process. (b) Corresponds to photoabsorption accompanied by a virtual plasmon process. (c) Shows the same process along with a real plasmon excitation.

Let us show that the minimum plasmon energy $\omega_p(k)$ required to make the above process real is $\omega_p(k) = \omega_p^c$ (or $k = k_c$). Let $\epsilon_p = p^2/2m$ and $\epsilon_{|\vec{p}-\vec{k}|} = (\vec{p}-\vec{k})^2/2m$ be the energies of the electron in the intermediate state and the final state, respectively. The conservation of energy between these two states requires that $\epsilon_p = \epsilon_{|\vec{p}-\vec{k}|} + \omega(k)$ or $\omega(k) = -k^2 + 2\vec{p}\cdot\vec{k}$ (hereafter we let $2m = 1$). This implies that k and $\omega(k)$ must satisfy the condition

$$\omega < -k^2 + 2pk \,. \tag{1}$$

Because of the Pauli principle satisfied by the conduction electron, another condition on the final-state electron is $\epsilon_{|\vec{p}-\vec{k}|} > \epsilon_F$, or using (1)

$$p^2 - \omega > k_F^2 \,. \tag{2}$$

In order that both conditions (1) and (2) can be satisfied simultaneously, the frequency and momentum (ω, k) of the plasmon must lie inside the truncated parabola of the ω-k plane shown by the shaded area in Fig. 2. In this figure, the plasmon dispersion curve $\omega = \omega_p(k)$ is represented by the thick curve extending from point A to B. The two dashed parabolas satisfy the equation

$$\omega = k(k \pm 2p_F) \tag{3}$$

and define the area of the single pair excitations. Thus, the above conditions imply that for the production of a real plasmon, the plasmon curve must, at least partially, lie within the shaded parabola. Now as the energy of the incoming photon E increases from the x-ray absorption edge frequency E_F, so would the energy ϵ_p $(= p^2)$ of the

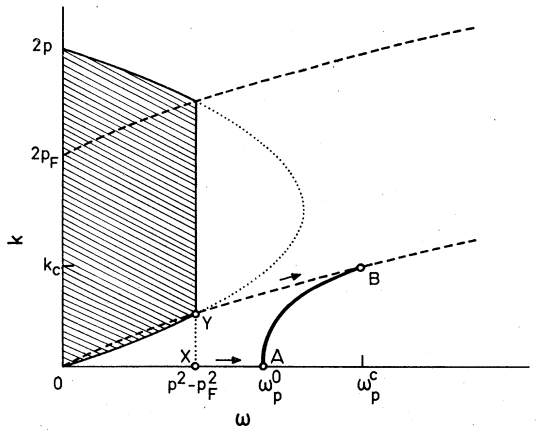

FIG. 2. Area within the dashed curves in the ω-k plane shows the region of single-particle excitation and the thick solid curve AB is the corresponding plasmon line. The shaded area inside the truncated parabola depicts the region where photoabsorption is accompanied by a real plasmon process.

ejected electron from ϵ_F ($=p_F^2$). This would, in turn, mean that the area under the shaded curve would increase, and the line joining the points X and Y in Fig. 2 would move to the right as the point Y would move along the dashed curve in the direction of the arrow. A plasmon production will become possible as soon as point X crosses point A. Obviously, this will occur when $\epsilon_p \geq \epsilon_F + \omega_p^0$ and this is exactly the process shown in Fig. 1(b). Note that at this stage curve AB does not yet entier the shaded area. The plasmon production is thus a virtual process at this frequency. Curve AB will enter the shaded area for a higher photon frequency, and consequently a higher ϵ_p. This will occur when point Y reaches point B and as indicated before, this is exactly the condition for the deexcitation of the ejected electron by a real plasmon process. This is what that has been described in Fig. 1(c). As it is obvious from Fig. 2, this condition is satisfied when $\epsilon_p = \epsilon_F + \omega_p^c$. These considerations make clear the critical role played by the frequency $E = E_F + \omega_p^c$ and why one expects to observe something unusual in the x-ray absorption spectrum at this frequency.

Since we do not consider multiplasmon transitions, the final state can be represented either by a state vector $|\vec{p}\rangle$ (zero-plasmon production) or by $|\vec{p}-\vec{k},\vec{k}\rangle$ (one-plasmon production). The above argument simply indicates that above a certain frequency, which we have shown to be $E_F + \omega_p^c$, these states can be degenerate. In other words, electron $\vec{p}$ can emit and reabsorb a plasmon $\vec{k}$; this corresponds to a resonance. However, the electronic levels have a finite width $\Gamma(\epsilon_p)$ due to damping by plasmon production. This width will damp the resonance, and the resonance will be spread over a few eV. At first sight it may appear that it would be hard to detect such a resonance. This would indeed by the case if we do not take into account the Fermi distribution discontinuity. Since the width $\Gamma(\epsilon_B)$ of the core state is much weaker than $\Gamma(\epsilon_p)$, this discontinuity, in fact, plays an essential role, making the final states available only if ϵ_p and $\epsilon_{|\vec{p}-\vec{k}|}$ are larger than ϵ_F. Actually it is the combined effect of these two widths which is responsible for the new plasmon structure that we are reporting in this paper.

III. SHAPE OF THE NEW STRUCTURE: SINGLE-PLASMON MODE

In the next section, we will undertake a detailed calculation of the x-ray photoabsorption in the first order theory of the effective electron-electron interaction. However, in order to obtain a feeling for the nature and shape of the predicted structure, in this section we discuss the x-ray absorption process within a simplified model of the electron-plasmon system. In this model we assume that the *only* plasmon mode which can be excited is the one having its wave vector $\vec{k}$ pointing in a small element $\Delta\vec{k}$. Such a model will also clearly indicate that the predicted structure is not a spurious effect due to some unphysical nature of the approximations of our theory and that the structure will be expected to persist *even in a renormalized theory*.

One of the terms contributing to the intensity of the x-ray absorption spectra of metals can be written as (see next section)

$$\mathcal{I}_A(E) = \frac{1}{\pi}\,\mathrm{Re}\int d\vec{p}\,|\Theta(\vec{p})|^2 \mathcal{S}(\vec{p},E)\,, \tag{4}$$

where $\Theta(\vec{p})$ represents the matrix element for x-ray absorption and where the frequency E is measured, as everywhere else in this paper, from the bottom of the conduction band. The actual frequency of the absorbed x-ray is thus $E-\epsilon_B$ where ϵ_B is the core hole (negative) energy.

In Eq. (4), $\mathcal{S}(\vec{p},E)$ is the renormalized propagator of the final-state electron which is excited from the core level by the x-ray absorption. This renormalized propagator has the form

$$\mathcal{S}(\vec{p},E) = \frac{i\theta(p-p_F)}{E-\epsilon_p-\Sigma(\mathrm{p},E)+i\lambda}\,, \tag{5}$$

where θ is the step function and where in the lowest order of effective Coulomb interaction the self-energy $\Sigma(\vec{p},E)$ can be expressed as[11,13]

$$\Sigma(\vec{p},E) = \frac{1}{(2\pi)^3}\int d\vec{k}\,\theta(|\vec{p}-\vec{k}|-p_F) \times V_+(\vec{k},E-\epsilon_{|\vec{p}-\vec{k}|})\,, \tag{6}$$

where $V_+(\vec{k},\omega)$ is that part of the effective interaction which is analytic in the upper half of the complex ω plane. Note that in this expression another term containing $\theta(p_F-|\vec{p}-\vec{k}|)V_-$ has been neglected since such a term would not contribute to the absorption process. Remembering that in this paper we are only interested in the plasmon production; we will only keep the plasmon part of V_+ which has the form[12,14,15]

$$V_+(\vec{k},\omega) = \tfrac{1}{2}v(\vec{k})\omega_p(\vec{k})c(\vec{k})\,\frac{\theta(k_c-k)}{\omega-\omega_p(\vec{k})+i\lambda}\,, \tag{7}$$

where $v(\vec{k})$ is the bare Coulomb potential $4\pi e^2/k^2$, $\omega_p(\vec{k})$ is the wave-number-dependent plasmon frequency (thick line in Fig. 2), and $c(\vec{k})$ is the weight factor determining the plasmon excitation and is determined from the sum rule[16]

$$\int_0^\infty d\omega\,\omega V_+^{\mathrm{tot}}(\vec{k},\omega) = -\tfrac{1}{2}\pi\,(\omega_p^0\epsilon_F)^2 V(\vec{k}) \tag{8}$$

applied to the total effective potential (plasmon

part + single pair part). One has $c(0)=1$ and $c(k_c)=0$. It is also found that $c(\mathrm{k})$ is practically equal to one for all plasmon wave numbers except in the region $k \leq k_c$ where it drops to zero very rapidly.

The electronic self-energy related to the plasmon excitation then has the form

$$\Sigma(p,E)=\frac{1}{2(2\pi)^3}\times\int d\vec{\mathrm{k}}\,\frac{v(\vec{\mathrm{k}})\omega_p(\vec{\mathrm{k}})c(\vec{\mathrm{k}})\,\theta(k_c-k)\,\theta(|\vec{\mathrm{p}}-\vec{\mathrm{k}}|-p_F)}{E-\epsilon_{|\vec{p}-\vec{k}|}-\omega_p(k)+i\lambda}. \tag{9}$$

and can be used in the propagator (5).

Let us now introduce our model and consider only the wave vector $\vec{\mathrm{k}}$ pointing in a small element $\Delta\vec{\mathrm{k}}$. It has a well-defined length and orientation with regard to the momentum $\vec{\mathrm{p}}$ of the electron. The electronic self-energy (9) for this particular model can be written

$$\Sigma_{\vec{k}}(p,E)=\frac{\Delta a_{\vec{k}}}{E-\epsilon_{p,k}+i\lambda}\,, \tag{10}$$

where

$$\epsilon_{p,k}=\epsilon_{|\vec{p}-\vec{k}|}+\omega_p(k) \tag{11}$$

and

$$\Delta a_{\vec{k}}=\frac{1}{2(2\pi)^3}\,v(\vec{\mathrm{k}})\omega_p(\vec{\mathrm{k}})c(\vec{\mathrm{k}})\Delta\vec{\mathrm{k}}\,. \tag{12}$$

With this simplified self-energy (10), the renormalized propagator (5) takes the form

$$\mathcal{S}(\vec{\mathrm{p}},E)=\frac{i(E-\epsilon_{p,k})}{(E-\epsilon_p+i\lambda)(E-\epsilon_{p,k}+i\lambda)-\Delta a_{\vec{k}}}\,, \tag{13}$$

where the θ functions have been dropped by assuming implicity that

$$p>p_F\,,\quad |\vec{\mathrm{p}}-\vec{\mathrm{k}}|>p_F\,,\quad \text{and } k<k_c$$

From the propagator (13), we can write the spectral function in the following form

$$\frac{1}{\pi}\,\mathrm{Re}\mathcal{S}(\vec{\mathrm{p}},E)=A^{+}_{\vec{p},\vec{k}}\,\delta(E-\nu^{+}_{\vec{p},\vec{k}})+A^{-}_{\vec{p},\vec{k}}\,\delta(E-\nu^{-}_{\vec{p},\vec{k}})\,, \tag{14}$$

where

$$A^{\pm}_{\vec{p},\vec{k}}=\tfrac{1}{2}\left[1\pm(\epsilon_p-\epsilon_{p,k})/R_{\vec{p},\vec{k}}\right]$$

and

$$\nu^{\pm}_{\vec{p},\vec{k}}=\tfrac{1}{2}(\epsilon_p+\epsilon_{p,k}\pm R_{\vec{p},\vec{k}})\,,$$

with

$$R_{\vec{p},\vec{k}}=[(\epsilon_p-\epsilon_{p,k})^2+4\Delta a_{\vec{k}}]^{1/2}\,.$$

This spectral function is directly related to cross section for absorption by Eq. (4). Thus, it gives the response of our one-plasmon model to a probe of frequency E.

It can be easily checked that for a small $\Delta a_{\vec{k}}$ (≈ 0) and for ϵ_p not very close to $\epsilon_{p,k}$, the spectral function (14) has a peak at the frequency $\nu^{0}_{\vec{p},\vec{k}} \equiv E \approx \epsilon_p$ (zero-plasmon excitation) with a probability

$$A^{0}_{\vec{p},\vec{k}}\ [\equiv A^{-}_{\vec{p},\vec{k}}(A^{+}_{\vec{p},\vec{k}})\ \text{for}\ \epsilon_p-\epsilon_{|\vec{p}-\vec{k}|}<(>)0]$$

which is practically one and that it gives another peak at $\nu^{1}_{\vec{p},\vec{k}} \equiv E \approx \epsilon_{p,k}$ (one-plasmon excitation) with a probability

$$A^{1}_{\vec{p},\vec{k}}\ [\equiv A^{+}_{\vec{p},\vec{k}}(A^{-}_{\vec{p},\vec{k}})\ \text{for}\ \epsilon_p-\epsilon_{|\vec{p}-\vec{k}|}<(>)0]$$

which is close to zero. Thus, the probability of x-ray photoabsorption with one-plasmon excitation is much weaker than the corresponding probability without plasmon excitation except in the vicinity of $\epsilon_{p,k}\approx\epsilon_p$. However, if $\epsilon_{p,k}\approx\epsilon_p$ i.e., if $\vec{\mathrm{p}}$ is such that the electron can excite the plasmon $\vec{\mathrm{k}}$ with conservation of energy the probabilities tend to be equal. In other words, as $\epsilon_{p,k}$ approaches ϵ_p, the probability $A^{0}_{\vec{p},\vec{k}}$ departs from one and $A^{1}_{\vec{p},\vec{k}}$ from zero and they become practiacally equal to each other when $\epsilon_{p,k}$ and ϵ_p are within the frequency range of $(\Delta a_{\vec{k}})^{1/2}$ (related to the electron damping). For $\epsilon_p=\epsilon_{p,k}$, one has the exact relationship $A^{0}_{\vec{p},\vec{k}}=A^{1}_{\vec{p},\vec{k}}=\frac{1}{2}$. We say that at this frequency the single-electron excitation process goes into a resonance with one-electron excitation accompanied by a plasmon process.

The above considerations are depicted in Fig. 3. In Fig. 3(a) the frequencies of the peaks are plotted as functions of the electron momentum p for the case $\Delta a_{\vec{k}}=0$ and are given by the two intersecting

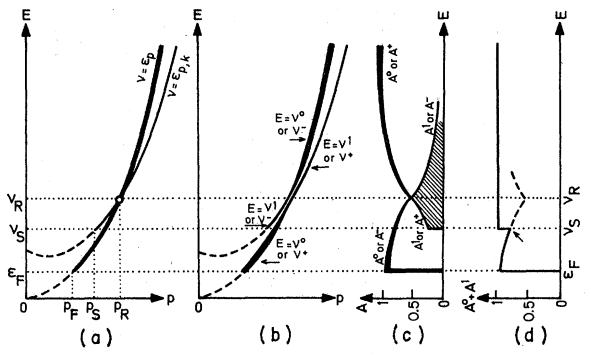

FIG. 3. Schematic representation of the nature and shape of the plasmon structure in a simplified electron-plasmon model (see text). (a) The intersecting parabolas are frequency peaks for zero plasmon (thick curve) and one plasmon processes plotted as functions of electron momentum $\vec{\mathrm{p}}$ with $\Delta a_k=0$. (b) Same curves as (a) for finite Δa_k. (c) The probabilities of the two processes are shown individually. (d) This figure represents the total probability.

parabolas. In Fig. 3(b) the same curves plotted with a finite $\Delta a_{\vec{k}}$. The widths of the curves in this figure represent the probabilities of the response for each frequency. These probabilities are shown separately in Fig. 3(c), as functions of frequency and the total probability obtained by adding the two is depicted in Fig. 3(d). [Note that if $\Delta a_{\vec{k}}$ goes to zero the curves $A^{\pm}_{\vec{p},\vec{k}}$ of Fig. 3(c) would tend to step functions].

The important point to realize now is the effect of the Fermi distribution. Since one must have $\epsilon_p > \epsilon_F$ and $\epsilon_{p,k} > \epsilon_F + \omega_p(\vec{k})$, the zero plasmon mode excitation curve must have a cutoff below ϵ_F and the one plasmon mode curve must have its cutoff below $\nu_s = \epsilon_F + \omega_p(k)$ as shown by the dotted curves in Figs. 3(a) and 3(b). This also corresponds to the origin of the low-frequency edges at frequency $E = \epsilon_F$ for the probability of an electron excitation without a plasmon production and at frequency $E = \epsilon_F + \omega_p(k)$ for the probability of an electron excitation with a plasmon production, as shown in Figs. 3(c) and 3(d). These edges are well known, in spite of the fact that the plasmon satellite edge was never observed at its minimum balue $\epsilon_F + \omega_p^0$. In general, the structure produced by the addition of the above two probabilities will be rather weak as shown in Fig. 3(d). But this edge may become quite important if ν_s is close to the resonance frequency $\nu_R \equiv \epsilon_p = \epsilon_{|\vec{p}-\vec{k}|} + \omega_p(k)$, since at this frequency the edge of the plasmon satellite is superposed on the cusp structure of the single-particle excitation probability $A^0_{\vec{p},\vec{k}}$. We may even hope to observe the isolated cusp structure of $A^0_{\vec{p},\vec{k}}$ if $\nu_s > \nu_R$. But by using the following phase space argument we can show that the condition $\nu_s > \nu_R$ can never be satisfied for any plasmon mode.

Since $\nu_s = p_F^2 + \omega_p(\vec{k})$, the maximum value of ν_s must be $\nu_s^{\max} = p_F^2 + \omega_p^c$. However, we have seen in Sec. II that the resonance condition $p^2 = \omega + |\vec{p} - \vec{k}|^2$ would be satisfied if the (ω, k) values lie in the shaded area of Fig. 2. The minimum value of the resonance momentum for which the shaded area enters the plasmon curve is determined by $p^2_{R\,\min} - p_F^2 = \omega_p^c$ (coincidence of Y and B). This shows that the minimum resonance frequency $\nu_R^{\min} \equiv p^2_{R\min} = \nu_s^{\max}$ i.e., ν_R must always be greater than ν_s. The same result could also be obtained by an analytic argument.

The conclusion of this section appears in Fig. 3(d). It shows that a structure would appear in the form of a dip at the frequency ν_s and would become particularly important when ν_s is close to ν_R i.e., when $\nu_s = \nu_R \approx \epsilon_F + \omega_p^c$. The next step is to proceed to a complete calculation of this structure in a realistic model where all $\vec{k}$ modes exist. This will be done in the next section in the first-order many-body perturbation theory.

IV. FIRST-ORDER THEORY

The calculation of the x-ray photoabsorption in the first-order effective Coulomb interaction can be performed using the same general lines as those of Ref. 8. Using Fermi's golden rule, the intensity of absorption can be written as

$$\mathcal{I}(E) = \frac{1}{\pi}\,\mathrm{Re}\int_0^\infty dt\, e^{i(E-\epsilon_B)t}\,\langle 0 \,|\, \Theta^\dagger(t)\Theta(0) \,|\, 0\rangle\ , \tag{15}$$

where Θ represents the dipolar operator and where the x-ray frequency E is measured from the bottom of the conduction band (see Fig. 1). Using a first-order diagrammatic expansion of (15) in the effective potential (7), we would obtain the diagrams of Fig. 4. These diagrams are related to the matrix element of (15) and give the four terms

$$\mathcal{I}(E) = \mathcal{I}_0(E) + \mathcal{I}_A(E) + \mathcal{I}_B(E) + \mathcal{I}_C(E)\,. \tag{16}$$

The important term by which the plasmon structure can be described and calculated is $\mathcal{I}_A(E)$(diagram A). However, we are also interested in the relative importance of the structure with regard to the whole spectrum. For this reason we have to use a reference intensity which will be provided by $\mathcal{I}_0$ (zeroth-order intensity). Moreover, we know that if we neglect any diagram or term contributing to a definite order, we miss the strong cancellation effects which validate the perturbative expansion. We have thus also to include diagrams B and C. We will also calculate the normalized intensity

$$I(E) = \mathcal{I}(E)/\mathcal{I}_0(E) \tag{17}$$

with $\mathcal{I}(E)$ given by (16). This expression allows us to estimate the importance of any many-body structure as a percentage of the local spectral intensity.

The rules to compute the diagrams of Fig. 4 are well known.[8] One associates, respectively, to the conduction-electron (solid) lines, to the core hole (double) lines and to the potential (dashed) lines

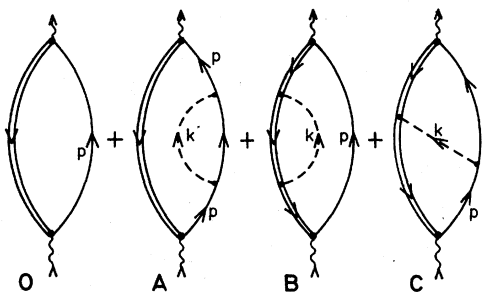

FIG. 4. Diagrams in zero-and first-order in effective Coulomb interaction contributing to the x-ray photoabsorption process.

the factors

$$\mathcal{S}(p, t_1 - t_2) = \theta(t_1 - t_2)\,\theta(p - p_F) e^{-i\epsilon_p (t_1 - t_2)},$$

$$\mathcal{S}_B(t_1 - t_2) = -\theta(t_2 - t_1) e^{-i\epsilon_B (t_1 - t_2)},$$

$$V_+(\vec{k}, t_1 - t_2) = (2\pi)^{-1} \int d\omega\, e^{-i\omega(t_1 - t_2)} V_+(k, \omega),$$

with $V_+(\vec{k}, \omega)$ given by (7). Factors

$$\Theta(p) = \langle \vec{p} \mid -i\vec{n} \cdot \vec{\nabla} \mid B \rangle$$

are associated to the radiation vertices (wavy lines of Fig. 4) ($\vec{n}$ is an averaged polarization vector); an overall minus sign takes into account the closed loop character of the diagrams. The above expressions are introduced in (15) (matrix element) and one integrates over times and momenta. In these calculations $\Theta(p)$ can be approximated by

$$\Theta(p) = D \text{ for } L \text{ bands}, \quad \Theta(p) = Dp \text{ for } K \text{ bands},$$

D being a constant.

Using the momenta labeled in Fig. 4, one obtains for the zeroth-order term

$$g_0(E) = \frac{D^2}{\pi} \int d\vec{p}\{p^2\} \operatorname{Re} \frac{i\theta(p - p_F)}{E - p^2 + i\lambda} = 2\pi D^2 \{E\} E^{1/2} \theta(E - \epsilon_F) \tag{18}$$

Here and below, the quantities within the curly brackets have to be replaced by 1 for L bands. This gives the well-known zeroth-order band shape in $E^{1/2}$ for L bands and $E^{3/2}$ for K bands. Similarly, one has for first-order terms

$$\begin{aligned} g_A(E) = &-\frac{D^2}{\pi(2\pi)^3} \int d\vec{k} \int d\vec{p}\{p^2\} \\ &\times \{\theta(|\vec{p} - \vec{k}| - p_F) \operatorname{Im} V_+(\vec{k}, E - \epsilon_{|\vec{p} - \vec{k}|}) \frac{\partial}{\partial \epsilon_p} \frac{\mathcal{P}}{E - \epsilon_p} \\ &+ \theta(p - p_F)[\theta(|\vec{p} - \vec{k}| - p_F) \operatorname{Re} V_+(\vec{k}, E - \epsilon_{|\vec{p} - \vec{k}|}) \\ &- \theta(p_F - |\vec{p} - \vec{k}|) \operatorname{Re} V_+(\vec{k}, \epsilon_{|\vec{p} - \vec{k}|} - E)] \\ &\times \pi \delta'(E - \epsilon_p)\}, \end{aligned}$$

$$\begin{aligned} g_B(E) = &-\frac{D^2}{\pi(2\pi)^3} \int d\vec{p}\{p^2\} \\ &\times \Big(\Theta(p - p_F) \operatorname{Im} V_+(\vec{k}, E - \epsilon_p) \frac{\partial}{\partial \epsilon_p} \frac{\mathcal{P}}{E - \epsilon_p} \\ &+ \operatorname{Re} V_+(\vec{k}, E - \epsilon_p) \pi \delta'(E - \epsilon_p)\Big), \end{aligned} \tag{19}$$

$$\begin{aligned} g_c(E) = &\frac{2D^2}{\pi(2\pi)^3} \int d\vec{k} \int dp (p^2 - \vec{p} \cdot \vec{k}) \\ &\times \Big(\theta(|\vec{p} - \vec{k}| - p_F) \operatorname{Im} V_+(\vec{k}, E - \epsilon_{|\vec{p} - \vec{k}|}) + \theta(p - p_F) \\ &\times [\theta(|\vec{p} - \vec{k}| - p_F) \operatorname{Re} V_+(\vec{k}, E - \epsilon_{|\vec{p} - \vec{k}|}) \\ &- \theta(p_F - |\vec{p} - \vec{k}|) \operatorname{Re} V_+(\vec{k}, \epsilon_{|\vec{p} - \vec{k}|} - E)] \\ &\times \frac{\mathcal{P}}{E - \epsilon_{|\vec{p} - \vec{k}|}} \delta(E - \epsilon_p)\Big). \end{aligned}$$

All the integrations contained in these expressions can be performed analytically except the last one, over $|\vec{k}|$, which has been computed numerically. For more details regarding these expressions we refer to Ref. 8 where we show, among other things, the way to handle those contributions to the matrix element of (15) which are proportional to t (shift of the whole spectrum). At this point, we would like to emphasize that the term that really describes the plasmon structure discussed in this paper, is the first term of g_A in Eq. (19). First, let us note (in the spirit of Sec. III) that g_A can be written in the form

$$g_A(E) = -\frac{D^2}{\pi} \int d\vec{p}\{p^2\} \operatorname{Im} \frac{\Sigma(p, E)}{E - \epsilon_p + i\lambda}$$

which is the first-order term in the expansion of

$$g_0(E) + g_A(E) + \cdots = \frac{D^2}{\pi} \int d\vec{p}\,\{p^2\} \times \operatorname{Re} \frac{i}{E - \epsilon_p - \Sigma(\vec{p}, E)}.$$

This latter expression is precisely the renormalized form of Eq. (18) and this is exactly the term that we had considered in Sec. III. Thus, the term in Eq. (19) that we should discuss in detail is the term containing $\operatorname{Im} V_+$. Using Eq. (8), it can be written more explicitly as

$$\begin{aligned} g'_A(E) = &\frac{D^2}{2\pi} \int_0^{k_c} dk\, k^2 c(k) v(k) \omega_p(k) \\ &\times \theta(E - \epsilon_F - \omega_p(k)) \\ &\times \left(\frac{\{E\}[E - \omega_p(k)]^{1/2}}{[k^2 + \omega_p(k)]^2 - 4k^2 E} + \frac{1}{4k} \ln\{A\}\right), \end{aligned}$$

where the second (smooth) logarithmic term appears only in the K bands (set $A = 1$ for L bands). The denominator of the first term cancels for

$$\omega_p(k) = -k^2 + 2kE^{1/2}.$$

Going back to the discussion of Sec. II we notice that it is precisely the condition required for the intersection of curves $0Y$ and AB of Fig. 2 (with $E = \epsilon_p$). The condition for the cancellation of the above denominator is thus that the photon has at least energy $E = E_F + \omega_p^c$. It is the reason why some peculiar behavior can be expected in the spectrum at this frequency. In fact, all the other first-order terms of Eq. (16) also have the same peculiar behavior at this frequency. Once the complete calculations are performed i.e., once the contributions from all the first-order terms are included, we obtain the curve of Fig. 5 for L, absorption spectra of Na, and that of Fig. 6 for the

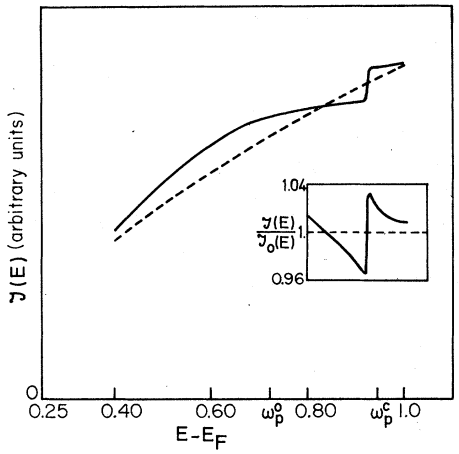

FIG. 5. L photoabsorption intensity of Na showing the structure due to plasmon production, near the frequency $E_F+\omega_p^c$. The dashed line represents the zeroth-order result. The inset shows the normalized intensity $I(E)$ defined by (17) near the plasmon structure.

K-absorption spectra of Mg. Let us note that in both cases, the structure appears in the form of a dip of 5%–7% near the frequency $E_F+\omega_p^c$ and that it extends over a frequency range of one or two electron volts. Our numberical computation also indicates that if the plasmon dispersion were not included, the structure would be much more pronounced and would appear at the frequency $E_F+\omega_p^0$.

V. CONCLUSIONS

In this paper, we have studied the effects of electron interactions on the x-ray photoabsorption spectra of metals in the framework of many-body perturbation theory. Our calculations predict the existence of a structure in the photoabsorption intensity due to excitation of a plasmon during the x-ray absorption process. It is shown that the structure is expected to occur at the frequency $E_F+\omega_p^c$, the cutoff frequency for plasmon production rather than at $E_F+\omega_p^0$, the threshold for plasmon excitation. This structure is not easy to observe primarily because it is weak and second, because it occurs in a spectral region where the band-structure effects are important. However, this structure is interesting because it is probably the only observable effect related to plasmon production in x-ray photoemission. Since the structure is supposed to occur at the frequency corresponding to the cutoff of plasmon, its observation would also give an experimental measure of the frequency extension in plasmon oscillations. It is interesting to note the Sénémaud has been able to observe this plasmon structure in the K spectra of Al and Mg at the expected frequencies (following paper).

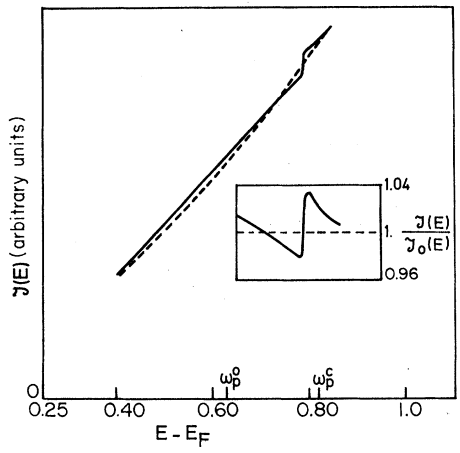

FIG. 6. K photoabsorption intensity of Mg. The plasmon structure appears near the frequency $E_F+\omega_p^c$. The dashed line represents the zeroth-order result. The inset shows the normalized intensity $I(E)$ defined by (17) near the plasmon structure.

Finally, we should perhaps make some comments regarding the validity of our approximations. The final calculations of Sec. IV have been carried out in the first-order perturbation theory. One thus has to make sure that the structure predicted is not spurious, appearing as an artifact of our approximations and that it will not be washed out by higher-order terms. In fact, we have already addressed this problem in Sec. III where it has been shown that the use of a renormalized propagator applied to a simplified model (where the plasmon has the momentum $\vec{k}$) exhibits the same structure. In this paper, we have also not included the contributions of the single-pair excitations explicitly. Such processes would contribute smoothly throughout the entire spectra without affecting the plasmon structure. In fact the plasmon contribution is not strictly limited to the the thick curve of Fig. 2. In a sense, the plasmon dispersion curve may be considered to penetrate slightly in the single pair region where there are remnants of a collective behavior. Function $\mathrm{Im}V_+$ still peaks strongly in the immediate continuation of the dispersion curve and this will not modify the results of our calculations significantly. Figure 2 shows that if we continue the dispersion curve slightly beyond the point B, the "extended" dispersion curve will still enter the shaded region when point Y reaches point B. The only differences will be (i) that the vertical sections of the calculated structure will be less steep. (ii) that the dip in the plasmon structure will be a bit more important.

This can be exhibited by slightly modifying the weight function $c(k)$ appearing in Eq. (7) and by making the cutoff momentum slightly larger than

k_c. We have seen this in our calculation by setting $c(k)$ equal to unity everywhere and the curves shown in Figs. 5 and 6 are, in fact, results of such a calculation. The curves obtained by using $c(k)$ given by Eq. (8) are very similar to those of Figs. 5 and 6 except that the strength of the plasmon structure appearing at frequency $E_F + \omega_p^c$ is between 3% to 5% for various metals. However, in view of above discussion we feel that the results shown in Figs. 5 and 6 are more realistic.

ACKNOWLEDGMENTS

We would like to thank Professor C. Bonnelle and Dr. C. Sénémaud for many interesting and useful conversations. We would also like to thank Professor P. Nozières for his comments regarding this work. This work was supported in part by the Fonds National de la Recherche Scientifique of Belgium and performed in the framework of the joint project ESIS (Electronic Structure in Solids) of the Universities of Liege and Antwerp.

*Permanent address: Dept. of Physics and Atmospheric Science, Drexel University, Philadelphia, Pa. 19104.

[1]R. A. Ferrell, Rev. Mod. Phys. 28, 308 (1956).
[2]F. Brouers, Phys. Lett. 11, 297 (1964); Phys. Status Solidi 11, K25 (1965).
[3]P. Longe and A. J. Glick, Phys. Rev. 177, 526 (1969).
[4]S. M. Bose and A. J. Glick, Phys. Rev. B 10, 3534 (1974).
[5]G. A. Rooke, Phys. Lett. 3, 234 (1963).
[6]H. Neddermeyer and G. Wiech, Phys. Lett. A 31, 17 (1970).
[7]C. Gähwiller and F. C. Brown, Phys. Rev. B 2, 1918 (1970).
[8]B. Bergersen, F. Brouers, and P. Longe, J. Phys. F 1, 945 (1971).
[9]J. Hubbard, Proc. R. Soc. A 243, 336 (1958).
[10]C. Sénémaud, (following paper), Phys. Rev. 18, 3929 (1978).
[11]S. M. Bose, A. Bardasis, A. J. Glick, D. Hone, and P. Longe, Phys. Rev. 155, 379 (1969).
[12]B. I. Lundqvist, Phys. Condens. Matter 6, 206 (1967); Phys. Condens. Matter. 7, 117 (1968).
[13]L. Hedin, Phys. Rev. 139, A796 (1965).
[14]A. W. Overhauser, Phys. Rev. B 3, 1888 (1970).
[15]A. J. Glick, in *Lectures on the Many-Body Problem, Naples*, 1060, edited by E. Caianiello (Academic, New York, 1962).
[16]A. J. Glick and R. A. Ferrell, Ann. Phys. (NY) 11, 359 (1960).